Inorganic Chemistry

ARTICLE

pubs.acs.org/IC

Microwave-Assisted Solvothermal Synthesis and Characterization of Metastable $LiFe_{1-x}(VO)_xPO_4$ Cathodes

Katharine L. Harrison and Arumugam Manthiram*

Electrochemical Energy Laboratory & Mechanical Engineering Program, The University of Texas at Austin, Austin, Texas 78712, United States

ABSTRACT: Vanadyl ion substituted $LiFePO_4$ cathodes of the form $LiFe_{1-x}(VO)_xPO_4$ for $0 \le x \le 0.25$ have been synthesized by a rapid microwave-solvothermal process at <300 °C within 10 min. Clear evidence of vanadyl ion substitution is demonstrated, despite a large size difference between Fe^{2+} and $(VO)^{2+}$, by characterizing the products structurally, spectroscopically, and electrochemically. The vanadyl ion substitution is accompanied by the formation of iron vacancies in the lattice and Fe_3O_4 impurity phase, which increases with increasing $(VO)^{2+}$ substitution for Fe^{2+} and could be removed with a magnetic stir bar. The formation of iron vacancies, along with the oxidation of some Fe^{2+} to Fe^{3+} to maintain charge neutrality, results in a decrease in the unit cell volume with increasing x despite the substitution of larger $(VO)^{2+}$ for Fe^{2+}. Charge−discharge data of the vanadyl ion substituted samples suggest suppression of the two-phase plateau behavior that is characteristic of $LiFePO_4$. Electrochemical data collected without any carbon coating reveal that the capacity and rate capability decreases, but the capacity retention improves with $(VO)^{2+}$ substitution.

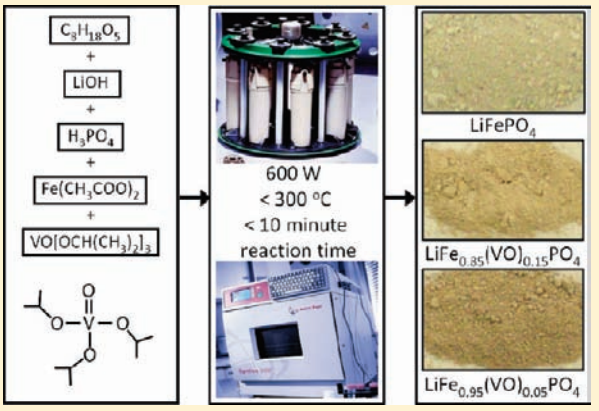

1. INTRODUCTION

Although lithium-ion batteries based on $LiCoO_2$ cathodes are being widely used in portable electronics, safety and toxicity concerns have led to demand for new cathode materials, especially for use in the transportation sector. Cathodes based on polyanions such as $Fe_2(SO_4)_3$ and $Fe_2(MoO_4)_3$ were first pursued by Manthiram and Goodenough in the late 1980s.[1,2] It was recognized that the covalently bonded polyanion groups lower the energy of redox couples through the inductive effect. This shifts the redox energy of couples like $Fe^{2+/3+}$ into a useful range. The covalently bonded polyanion groups also lead to higher thermal stability, which is a very important attribute for large battery packs. Several polyanion-based cathode materials have since then been developed, but of particular interest is the discovery of olivine $LiFePO_4$ by Padhi et al.[3] Since it was discovered in 1997, $LiFePO_4$ has been widely studied in the literature and has also been commercialized.[4−6]

$LiFePO_4$ is a particularly promising cathode material for lithium-ion batteries because iron is inexpensive, abundant, and environmentally benign. $LiFePO_4$ also has a high theoretical capacity of 170 mAh/g and a discharge plateau at 3.45 V vs Li/Li^+. Because of poor electronic and ionic conductivities, however, the high capacity can only be realized after coating $LiFePO_4$ with carbon or other conductive materials and by reducing the effective diffusion length by synthesizing small particle sizes.[7−17] Our group has recently demonstrated that $LiFePO_4$ can be synthesized at low temperatures (<300 °C) by a microwave-solvothermal (MW-ST) method.[13−17] This process results in single crystalline, uniform size $LiFePO_4$ nanorods and is advantageous for reducing energy consumption during synthesis as well as manufacturing cost.

Although $LiFePO_4$ is the most promising of the polyanion cathodes to date, there are several other candidate polyanion cathode materials, including $LiVOPO_4$, which have been studied to a much lesser extent than $LiFePO_4$. With a slightly lower theoretical capacity than $LiFePO_4$ (159 mAh/g) but with a higher voltage (3.7−4.0 V vs Li depending on the phase), $LiVOPO_4$ offers higher theoretical energy density than $LiFePO_4$.[18−24] However, vanadium is toxic and more expensive than iron, so $LiFePO_4$ may always remain more desirable as a cathode material than $LiVOPO_4$. Regardless, we were interested in substituting the vanadyl (VO^{2+}) ion for Fe^{2+} in $LiFePO_4$ for the purpose of increasing energy density and understanding the crystal chemistry.

$LiVOPO_4$ forms several different phases, but olivine $LiVOPO_4$ has not been successfully synthesized, which means that $LiVOPO_4$ and $LiFePO_4$ do not have the same structure.[18−20] However, $LiFePO_4$ and the β phase of $LiVOPO_4$ both belong to the space group *Pnma* and have three-dimensional structures consisting of channels for lithium removal and insertion during the charge and discharge process.[5,6,18,21−23] Figure 1 compares the structures of $LiFePO_4$ and β-$LiVOPO_4$. Since the structures of

Received: December 27, 2010
Published: March 07, 2011

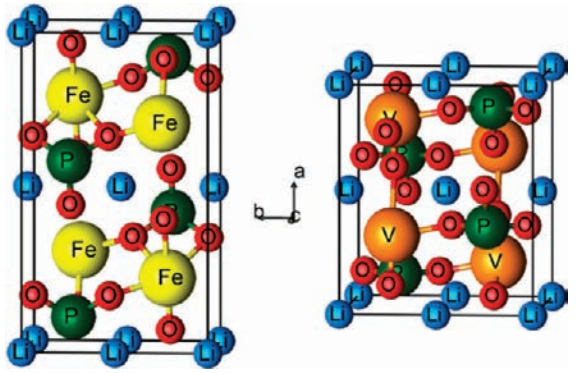

Figure 1. Crystal structures of $LiFePO_4$ (left) and β-$LiVOPO_4$ (right).

$LiFePO_4$ and β-$LiVOPO_4$ are different and the vanadyl ion is larger than the iron ion, it may be difficult to form vanadyl substituted $LiFePO_4$ by conventional high-temperature synthesis processes. Interestingly, owing to the low synthesis temperatures involved, the microwave-assisted synthesis could lead to metastable phases that are not otherwise accessible. Accordingly, we have extended the MW-ST process to synthesize vanadyl substituted $LiFePO_4$ with the formula $LiFe_{1-x}(VO)_xPO_4$ for $0 \leq x \leq 0.25$ and $x = 1$. These samples were synthesized to study the crystal chemistry and to determine if the energy density of $LiFePO_4$ could be improved because of the redox behavior of the vanadyl ion, which is higher in potential than the iron ion. Furthermore, similar to $LiFePO_4$, the rate capability of $LiVOPO_4$ can be improved by decreasing the particle size.[19] Thus, MW-ST synthesis could be a promising method to make $LiVOPO_4$ since the particle size in the MW-ST process can be tuned easily to create nanoparticles of different sizes.[16]

2. EXPERIMENTAL SECTION

2.1. Microwave Solvothermal Synthesis. $LiFe_{1-x}(VO)_xPO_4$ samples were synthesized by a rapid MW-ST method. Stoichiometric ratios of lithium hydroxide (Fisher), iron acetate (STREM), phosphoric acid (Fisher), and vanadium tri-isopropoxide oxide ($VO(OC_3H_7)_3$, Alfa Aesar) precursors were dissolved in tetraethylene glycol (Alfa Aesar) to obtain $LiFe_{1-x}(VO)_xPO_4$ with $0 \leq x \leq 0.25$ and $x = 1$. The resulting brown (for $0 \leq x \leq 0.25$) and red (for $x = 1$) solutions were transferred and sealed in high pressure quartz vessels. These vessels were secured on a rotor which was placed on a turntable in a microwave reaction system (Anton Paar Synthos 3000). The turntable was spun during synthesis to ensure uniform microwave heating, and stir bars were placed in each vessel to obtain uniform reactant mixing. The power was programmed to a constant level of 600 W. It took 20−30 min to ramp the temperature up to 260 °C, at which point the products formed. After reaching 260 °C, the constant power of 600 W was applied for 5−10 additional min, during which time the temperature remained between 260 and 280 °C. The temperatures of the vessels were monitored by infrared temperature sensors. The pressure was also monitored and was always kept below 30 bar throughout the synthesis. Because the particle size is dependent on the concentration of the precursors, the concentrations of lithium and phosphate ions were kept constant at 0.17 M. After synthesis, the microwave system went into convective cooling mode, and when the temperature was below 50 °C, the vessels were removed. A schematic of the synthesis process is depicted in Figure 2.

The magnetic stir bars in the vessels had varying amounts of a dark brown powder impurity stuck to them after syntheses of the $LiFe_{1-x}(VO)_xPO_4$ samples. This impurity was removed by stirring the solution

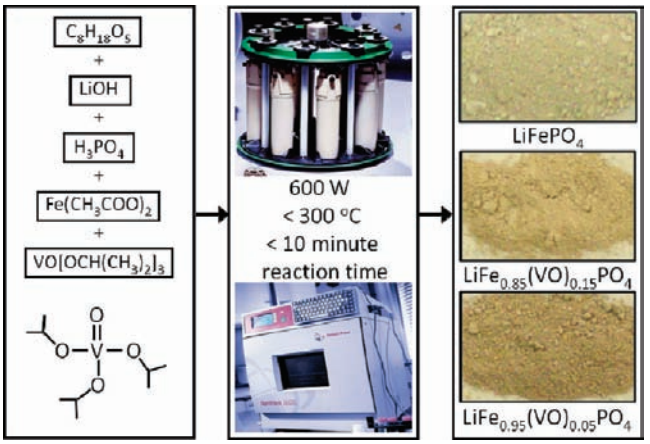

Figure 2. Illustration of the microwave-solvothermal synthesis of $LiFe_{1-x}(VO)_xPO_4$.

repeatedly with a magnetic rod until the rod came out of the solution clean. The amount of magnetic impurity increased with increasing x in $LiFe_{1-x}(VO)_xPO_4$. The magnetic impurity was collected, dried, and analyzed by X-ray diffraction (XRD). It was identified as Fe_3O_4 (magnetite).

The Fe_3O_4 impurity was present despite careful analysis to ensure that the precursors were added to the solution in the intended ratios. Thermogravimetric analysis (TGA) and inductively coupled plasma (ICP) analysis were utilized to determine the water content of the iron acetate and lithium hydroxide precursors. The TGA and ICP results agreed with each other within 2%. The phosphoric acid precursor concentration was confirmed by ICP and acid−base titration, which also agreed within 2%. The vanadium tri-isopropoxide oxide concentration was also confirmed by ICP. Adjusting amounts of precursors based on the ICP and TGA data ensured that the correct concentrations were being added to the reactant solutions.

After removing the Fe_3O_4 impurity, the precipitates were washed with acetone and centrifuged several times until the decanted solution was clear. Then the products were dried overnight at 160 °C in a vacuum oven. The $LiFePO_4$ powder was light gray in color, and the $LiFe_{1-x}(VO)_xPO_4$ compositions were gray with an increasingly brownish-pink tint with increasing $(VO)^{2+}$ substitution. The $LiVOPO_4$ sample was reddish-brown in color.

2.2. Sol−Gel Synthesis of β-$LiVOPO_4$. The $LiVOPO_4$ prepared by the MW-ST method was found to be amorphous, so β-$LiVOPO_4$ was also synthesized by a sol−gel (SG) method[24] for use as a comparison in FTIR and X-ray photoelectron spectroscopy (XPS) experiments. The sol−gel synthesized $LiVOPO_4$ will hereafter be referred to as SG $LiVOPO_4$ so as to not be confused with microwave products. To prepare the SG $LiVOPO_4$, V_2O_5 (Alfa Aesar) and oxalic acid (Fisher) were dissolved in water in a 1:3 ratio and stirred at 70 °C until the solution turned blue. Lithium nitrate (Acros Organics) and ammonium dihydrogen phosphate (Acros Organics) were then added, and the resulting solution was stirred for 4 h. The solution was then dried in an air oven at 100 °C until a green powder was formed. The powder was heated in air at 300 °C for 4 h and then at 500 °C for 4 h. The relevant reactions are given below.[24]

$$V_2O_5 + 3H_2C_2O_4 \rightarrow 2VOC_2O_4 + 3H_2O + CO_2 \quad (1)$$

$$VOC_2O_4 + LiNO_3 + NH_4H_2PO_4 \rightarrow LiVOPO_4 + 2CO + 2NO + 3H_2O \quad (2)$$

2.3. Structural, Physical, Chemical, and Spectroscopic Characterizations. XRD was performed on a Philips X-ray diffractometer

dx.doi.org/10.1021/ic1025747 |Inorg. Chem. 2011, 50, 3613–3620

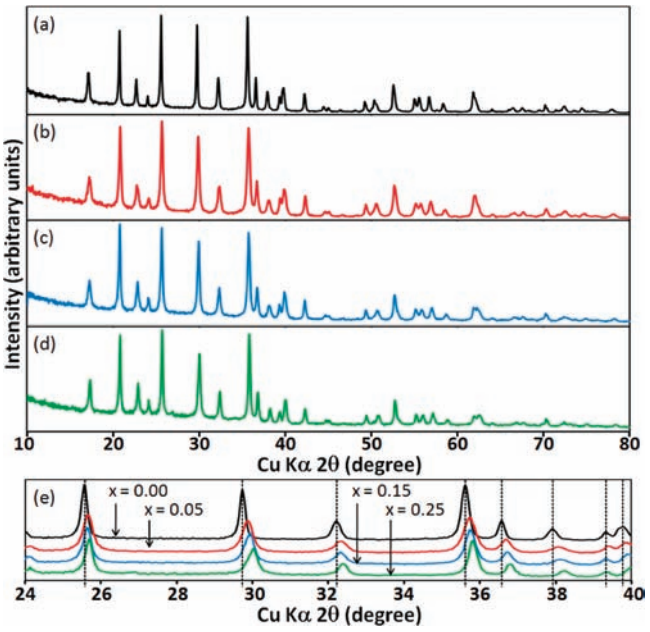

Figure 3. XRD patterns of (a) $LiFePO_4$, (b) $LiFe_{0.95}(VO)_{0.05}PO_4$, (c) $LiFe_{0.85}(VO)_{0.15}PO_4$, and (d) $LiFe_{0.75}(VO)_{0.25}PO_4$, and (e) a comparison of several $LiFe_{1-x}(VO)_xPO_4$ patterns over a smaller 2θ range.

with filtered Cu Kα radiation, and scanning electron microscopy (SEM) images were obtained with a LEO 1530 SEM. Fourier Transform Infrared (FTIR) spectra were collected with a PerkinElmer BX FTIR spectrometer. Pellets for FTIR analysis were prepared by grinding and pressing samples with dried KBr powder. A Varian 715-ES ICP optical emission spectrometer was used for elemental analysis. XPS spectra were acquired by a Kratos AXIS Ultra DLD machine with monochromatic Al Kα radiation. The pass energy was set to 20 eV, and automatic charge neutralization was used for all samples. Carbon spectra were collected for each sample, and the peaks were shifted such that the largest carbon peak was centered at 284.5 eV. Sputtering was done on the SG $LiVOPO_4$ sample at a beam energy of 4 keV for 50 s leading to an estimated 3 nm of material removal. Peak fitting was performed using CasaXPS software with Shirley type background removal and 30% Gaussian−70% Lorentzian curves.

2.4. Electrochemical Characterization. Cathodes were prepared by grinding 75 wt % active material with 12.5 wt % conductive carbon and 12.5 wt % teflonated acetylene black (TAB) in a mortar and pestle. TAB consists of polytetrafluoroethylene (PTFE) and acetylene black. The resulting composites were rolled into thin sheets and cut into 0.64 cm^2 area circles using a punch. The electrodes had approximately 7 mg of active material and were dried overnight in a vacuum oven at 115 °C before constructing cells. CR2032 coin cells were assembled in an argon filled glovebox using a metallic lithium anode, Celgard polypropylene separators, and 1 M $LiPF_6$ in 1:1 diethyl carbonate/ethylene carbonate as the electrolyte.

The coin cells were cycled on an Arbin battery cycler within a range of 2.0−4.3 V for the $LiFe_{1-x}(VO)_xPO_4$ samples. SG $LiVOPO_4$ was cycled in the range of 2.0−4.3 V to be consistent with the rest of the study, but it was also cycled between 3.0 and 4.5 V since that is the typical range for $LiVOPO_4$. Open-circuit voltage curves were collected by charging the cells at a C/50 rate in small increments. After each increment, the cell was left at open circuit until the voltage was stable. Voltage stability generally was achieved after resting at open circuit for several days to weeks depending on the state of charge. Cyclic voltammetry data was obtained using a two electrode coin cell assembly on a Radiometer Analytical Voltalab PGZ402 Potentiostat with a step of 0.1 mV/s.

Table 1. Lattice Parameters of $LiFe_{1-x}(VO)_xPO_4$ with $0 \leq x \leq 0.25$

compound	a (Å)	b (Å)	c (Å)	volume (Å^3)
$x = 0.0$	10.326(15)	5.98(2)	4.694(9)	289.85
$x = 0.05$	10.299(19)	5.965(14)	4.685(9)	287.82
$x = 0.10$	10.281(16)	5.962(12)	4.687(8)	287.29
$x = 0.15$	10.28(2)	5.944(16)	4.687(11)	286.40
$x = 0.25$	10.245(19)	5.932(10)	4.693(10)	285.21

Table 2. Elemental Ratios Obtained from ICP Analysis of $LiFe_{1-x}(VO)_xPO_4$ ($0 \leq x \leq 0.25$)

compound	Fe/P	V/P	Li/P
$LiFePO_4$	0.99		1.00
$LiFe_{0.95}(VO)_{0.05}PO_4$	0.96	0.05	0.99
$LiFe_{0.90}(VO)_{0.10}PO_4$	0.86	0.10	0.97
$LiFe_{0.85}(VO)_{0.15}PO_4$	0.77	0.16	1.02
$LiFe_{0.75}(VO)_{0.25}PO_4$	0.70	0.24	0.99

3. RESULTS AND DISCUSSION

3.1. XRD and ICP Characterizations. XRD patterns for the $LiFe_{1-x}(VO)_xPO_4$ materials are shown in Figure 3a−d for $0 \leq x \leq 0.25$. The $LiFe_{1-x}(VO)_xPO_4$ patterns resemble the $LiFePO_4$ pattern very closely. Impurity peaks for Fe_3O_4 are not detectable, demonstrating that the impurity has been adequately removed by stirring with a magnetic bar, as discussed previously. Figure 3e compares the patterns for the $LiFe_{1-x}(VO)_xPO_4$ samples over a smaller range of 2θ to demonstrate the clear shift to higher angles with increasing x in $LiFe_{1-x}(VO)_xPO_4$ and to illustrate the lack of impurities. Table 1 gives the lattice parameter values of the samples. It is clear that there is a systematic decrease in unit cell volume with increasing $(VO)^{2+}$ substitution for Fe^{2+}. Since the $(VO)^{2+}$ ion is larger than Fe^{2+}, one would expect an opposite trend, that is, one would anticipate the unit cell volume to steadily increase with increasing $(VO)^{2+}$ substitution. This contradictory behavior can be explained by examining the ICP results given in Table 2 for the vanadyl ion substituted samples.

Table 2 clearly shows that the V/P ratios are nominally equal to the expected ratios for the intended samples. Similarly, the Li/P ratios are close to unity for all of the vanadyl ion substituted samples, as expected. However, substitution of more than 5 mol percent of $(VO)^{2+}$ for Fe^{2+} results in consistently lower Fe/P ratios than expected.

Stoichiometric amounts of precursors were mixed to form each of the samples according to the formula $LiFe_{1-x}(VO)_xPO_4$. As discussed earlier, great care was taken to ensure that the precursors were added in the intended ratios. Despite this, as the value of x increased in $LiFe_{1-x}(VO)_xPO_4$, increasing amounts of Fe_3O_4 impurity were formed, and they were removed from the synthesis products.

These observations suggest that the lattice can only incorporate a small amount of $(VO)^{2+}$ for Fe^{2+} before iron vacancies form. The excess iron in solution that cannot be incorporated into the lattice forms Fe_3O_4. Even when synthesizing pristine $LiFePO_4$, excess iron acetate leads to the formation of Fe_3O_4. This has been tested by synthesizing $LiFePO_4$ with 5%, 10%, and 15% excess iron acetate. ICP analysis confirms that the excess iron does not wash out of solution and remains in ratios proportional to the amount of extra iron precursor taken in the reaction

dx.doi.org/10.1021/ic1025747 |Inorg. Chem. 2011, 50, 3613–3620

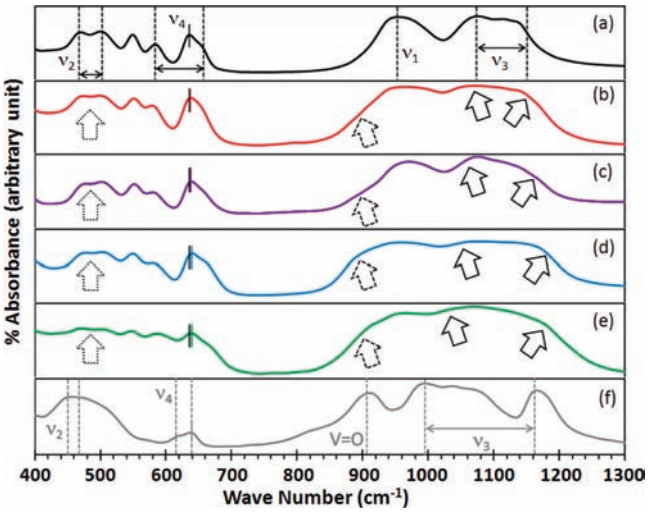

Figure 4. FTIR spectra of (a) $LiFePO_4$, (b) $LiFe_{0.95}(VO)_{0.05}PO_4$, (c) $LiFe_{0.90}(VO)_{0.10}PO_4$, (d) $LiFe_{0.85}(VO)_{0.15}PO_4$, (e) $LiFe_{0.75}(VO)_{0.25}PO_4$, and (f) SG $LiVOPO_4$.

mixture. XRD confirms that the excess iron is in the form of Fe_3O_4.

For the $LiFe_{1-x}(VO)_xPO_4$ samples, we believe that iron vacancies are formed, and the excess iron acetate in solution in turn forms Fe_3O_4. The iron vacancies explain why the unit cell volume decreases, rather than increases, with increasing x in $LiFe_{1-x}(VO)_xPO_4$. Even though $(VO)^{2+}$ is larger than Fe^{2+}, the unit cell volume decreases because iron vacancies, and the corresponding oxidation of some larger Fe^{2+} to smaller Fe^{3+} to compensate for the charge imbalance, cause the unit cell to contract. Furthermore, the formation of iron vacancies could help to accommodate the larger VO^{2+} ions in the lattice.

3.2. FTIR Characterization. Although it is unclear exactly how iron vacancies may be distributed and how the $(VO)^{2+}$ ions arrange themselves in the lattice, XRD data clearly suggest vanadyl ion substitution rather than a two-phase mixture or coating. Further evidence of vanadyl ion incorporation into the lattice is provided by the FTIR data shown in Figure 4. The FTIR spectra for $LiFePO_4$ and SG $LiVOPO_4$ are consistent with the spectra found in the literature.[25−27] Because bands in the FTIR spectra arise primarily from bending and stretching modes of the PO_4^{3-} groups, the spectrum of SG $LiVOPO_4$ is not vastly different from that for $LiFePO_4$.

IR spectra of the $LiFe_{1-x}(VO)_xPO_4$ samples closely resemble the $LiFePO_4$ spectrum, but have several features which shift toward the SG $LiVOPO_4$ spectrum with increasing x. The asymmetric stretching modes of the P−O bond are between $\nu_2 = 468$ and $\nu_2 = 503$ cm^{-1} for $LiFePO_4$ and are between $\nu_2 = 453$ and $\nu_2 = 467$ cm^{-1} for SG $LiVOPO_4$. As x increases in $LiFe_{1-x}(VO)_xPO_4$, the $LiFePO_4$ doublet becomes less pronounced and the curves flatten in the ν_2 region, as illustrated by the dotted line arrows in Figure 4. The flatter profile in this region shows more resemblance to the SG $LiVOPO_4$ spectrum. A similar pattern is seen for the asymmetric bending modes of the O−P—O bond, which are in the regions between $\nu_4 = 583$ and $\nu_4 = 652$ cm^{-1} for $LiFePO_4$ and between $\nu_4 = 619$ and $\nu_4 = 637$ cm^{-1} for $LiVOPO_4$. In particular, obvious shifting is seen as the vanadyl ion is substituted for iron in the peak at $\nu_4 = 635$ cm^{-1} for $LiFePO_4$. As x increases in $LiFe_{1-x}(VO)_xPO_4$, the peaks move toward the peak for $LiVOPO_4$ at $\nu_4 = 637$ cm^{-1}. This is indicated by the solid, colored lines in Figure 4, and a black line indicating the peak position for $LiFePO_4$ is shown on each plot for a comparison.

There is also a peak associated with the V═O bond in the SG $LiVOPO_4$ spectrum at $\nu = 909$ cm^{-1}. The broad peak between $\nu_1 = 944$ and $\nu_1 = 962$ cm^{-1} for $LiFePO_4$ (which is a symmetric stretching vibration) extends to lower frequencies, and the plateau between 680 and 880 cm^{-1} gradually shrinks as x increases in $LiFe_{1-x}(VO)_xPO_4$. The shrinking plateau, illustrated by the dotted line arrows in Figure 4, is due to the influence of the V═O bond in the samples and should be at around 909 cm^{-1}. Furthermore, $LiFePO_4$ has antisymmetric stretching modes of the P−O bond between $\nu_3 = 1078$ and $\nu_3 = 1134$ cm^{-1}, and $LiVOPO_4$ has comparable modes over a much wider range between $\nu_3 = 996$ and $\nu_3 = 1166$ cm^{-1}. Correspondingly, as x increases in $LiFe_{1-x}(VO)_xPO_4$, the ν_3 peaks occur over an increasingly larger range than for $LiFePO_4$. This is illustrated by the solid line arrows in Figure 4. These features are all consistent with vanadyl ion substitution for iron in $LiFePO_4$.

It should be noted that in attempting to synthesize $LiFe_{1-x}(VO)_xPO_4$, it might also be possible for V^{5+} to substitute in the anion site for P^{5+} rather than the cation site, leading to VO_4^{3-} ions. Because the FTIR spectra is so dominated by the polyanion group, we would expect to see large differences in the spectra if $LiFeP_{1-x}V_xO_4$ is formed, rather than only the small shifts evident in Figure 4. For example, the FTIR spectra of $LiCoVO_4$ and $LiNiVO_4$ look very different from that of $LiFePO_4$.[28,29] Therefore, the small shifts evident from Figure 4 are more consistent with cation substitution than with anion substitution. Also, attempts to mix precursors in stoichiometric ratios to form $LiFeV_xP_{1-x}O_4$ resulted in much higher amounts of Fe_3O_4 impurity, which further leads us to believe that $LiFe_{1-x}(VO)_xPO_4$ rather than $LiFeV_xP_{1-x}O_4$ is formed. Additionally, the substituted cation should be the vanadyl ion rather than a vanadium ion because the vanadium tri-isopropoxide oxide precursor used (structure shown in Figure 2) contains a very strong V═O, which is unlikely to be broken during the synthesis.

3.3. XPS Characterization. Although the oxidation state of vanadium in the vanadium tri-isopropoxide oxide precursor used in this study is 5+, tetraethylene glycol is capable of reducing V^{5+} to V^{4+}. This is verified by the XPS data shown in Figure 5. The vanadium peaks are shown in Figure 5a for MW-ST $LiFe_{0.85}(VO)_{0.15}PO_4$ and SG $LiVOPO_4$. It is first necessary to analyze the peaks for SG $LiVOPO_4$ to determine the expected peak locations for $V^{4+/5+}$ in the vanadyl ion. The $2p_{1/2}$ and $2p_{3/2}$ peaks for the SG $LiVOPO_4$ sample were not well fit with single peaks, so two peaks were used for each core line. The two peaks for the $2p_{3/2}$ electrons were at binding energies of 516.5 and 517.1 eV. To our knowledge, there is no XPS data for vanadium in β-$LiVOPO_4$, so the identification of the peaks can only be approximated by comparing to vanadium binding energies in other materials. The binding energies for V^{3+}, V^{4+}, and V^{5+} differ by only about 1.5 eV, and literature values vary significantly. This is compounded by the fact that some researchers shift their peaks so that the carbon 1s peak is at 284.5 eV, some shift carbon to 285.0 eV, and others shift the oxygen peaks to a certain value to standardize the measurements. Silversmit et al.[30] compared several vanadium oxidation states among various studies and included their standardization conditions. The average value among the studies they examined were 517.2 eV for V^{5+} in V_2O_5 and 516.0 for V^{4+} in VO_2. The peaks at 516.5 and 517.1 eV

dx.doi.org/10.1021/ic1025747 |Inorg. Chem. 2011, 50, 3613–3620

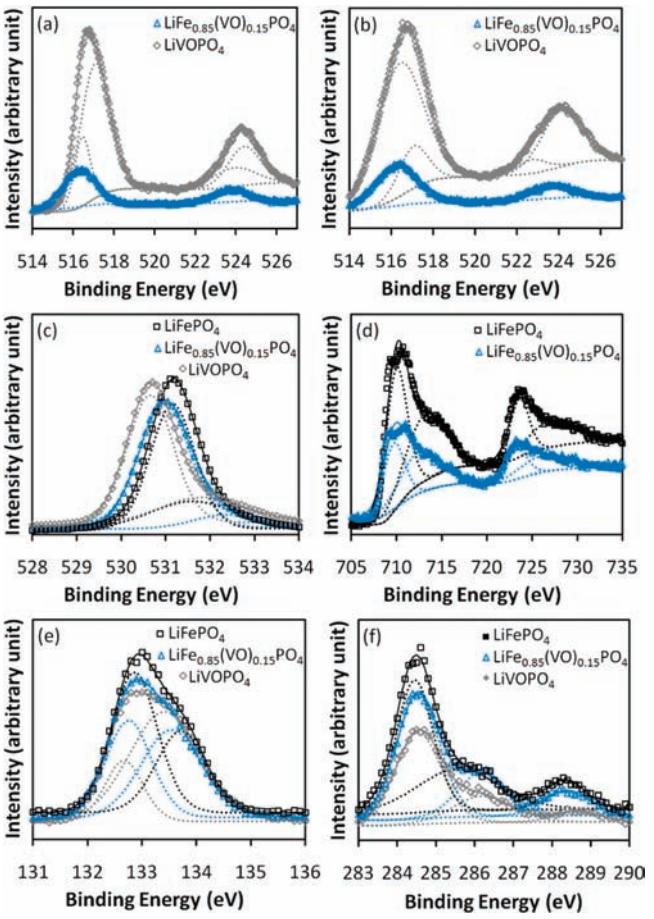

Figure 5. XPS data of $LiFe_{1-x}(VO)_xPO_4$: (a) V 2p, (b) V 2p sputtered, (c) O 1s, (d) Fe 2p, (e) P 2p, and (f) C 1s. Large symbols indicate raw data, dots correspond to the various peak fits to the data, and solid lines correspond to the sum of the peak fits.

in the SG $LiVOPO_4$ sample agree reasonably with the average V^{4+} and V^{5+} values in Silversmit et al.[30] Titration of the SG $LiVOPO_4$ sample against potassium permanganate confirmed an oxidation state of 4.10 for the vanadium in the SG $LiVOPO_4$ sample, further suggesting a combination of V^{4+} and V^{5+} oxidation states. As shown in Figure 5b, sputtering the sample led to an increase in the amplitude of the peak for V^{4+} and a decrease in the peak for V^{5+}. This suggests that the peak for V^{5+} is present because of surface oxidation of the vanadium.

The $2p_{1/2}$ and $2p_{3/2}$ peaks for $LiFe_{0.85}(VO)_{0.15}PO_4$ were easily fit to single peaks. The $2p_{3/2}$ peak was located at 516.5 eV. This agrees well with the location of the V^{4+} peak for the SG $LiVOPO_4$ sample and corroborates our claim that we have substituted $(VO)^{2+}$ for Fe^{2+} rather than VO_4^{3-} for PO_4^{3-} because we have an oxidation state of V^{4+} rather than V^{5+} for $LiFe_{0.85}(VO)_{0.15}PO_4$. Furthermore, the V/P ratio on the surface of the $LiFe_{0.85}(VO)_{0.15}PO_4$ sample was found to be V/P = 0.16. This value agrees well with the intended V/P ratio and also agrees well with the bulk V/P ratio determined by the ICP analysis. This shows that the vanadium is not a surface coating; rather, the vanadyl ion substitutes uniformly for iron in the olivine lattice.

Examination of the oxygen peaks provides further evidence of vanadyl ion substitution into $LiFePO_4$. The oxygen data were all fit to two peaks, as shown in Figure 5c. The large oxygen peak for $LiFePO_4$ agrees well with literature values, and the smaller peaks

Table 3. XPS Binding Energies (eV) of $LiFe_{1-x}(VO)_xPO_4$

	V	V	O	P	P	Fe	Fe
compound	$2p_{3/2}$	$2p_{1/2}$	1s	$2p_{3/2}$	$2p_{1/2}$	$2p_{3/2}$	$2p_{1/2}$
$LiFePO_4$			531.6	132.9	133.7	710.1	723.7
						713.6	727.5
$LiFe_{0.85}(VO)_{0.15}PO_4$	516.5	523.8	531.0	132.9	133.6	709.8	723.4
						712.9	726.8
SG $LiVOPO_4$	516.5	523.9	530.7	132.7	133.4		
	517.1	524.4					

in the oxygen spectra are generally attributed to surface contamination.[31,32] The main peak for $LiFe_{0.85}(VO)_{0.15}PO_4$ is centered between the $LiFePO_4$ and $LiVOPO_4$ peaks, as summarized in Table 3. The shift in the oxygen peak relative to $LiFePO_4$ is likely due to the influence of oxygen in the vanadyl ion; the electrons from the oxide ions in $LiFe_{0.85}(VO)_{0.15}PO_4$ are ejected at slightly different energies than in pure $LiFePO_4$ because the chemical environment has been altered by the presence of $(VO)^{2+}$. Shifts in the oxygen peaks for $LiFe_{0.85}(VO)_{0.15}PO_4$ from the $LiFePO_4$ peak locations toward the SG $LiVOPO_4$ peak locations are indicative of vanadyl ion substitution for iron in $LiFePO_4$.

The $2p_{1/2}$ and $2p_{3/2}$ iron peaks are shown in Figure 5d, each of which were fitted to two peaks. The iron peaks for $LiFePO_4$ at 710.1 and 723.7 eV agree well with the literature values for Fe^{2+}, and the peaks at 713.6 and 727.5 eV agree well with the literature values for Fe^{3+}.[33,34] The presence of Fe^{3+} is likely due to surface oxidation. The peaks for $LiFe_{0.85}(VO)_{0.15}PO_4$ are at similar locations to those for $LiFePO_4$, but are shifted slightly to lower binding energies, likely because of the different chemical environment imposed by $(VO)^{2+}$ substitution and vacancies in the Fe^{2+} site.

The phosphorus data for $LiFePO_4$, shown in Figure 5e, was fit to two peaks corresponding to the $2p_{1/2}$ and $2p_{3/2}$ core lines as is consistent with the literature,[33,34] and the peaks for $LiFe_{0.85}(VO)_{0.15}PO_4$ were found to be in the same locations as for $LiFePO_4$. The phosphorus peak locations for $LiFePO_4$ and $LiVOPO_4$ are in very similar locations, so it is as expected that the $LiFe_{0.85}(VO)_{0.15}PO_4$ peaks were not shifted from the $LiFePO_4$ peaks. Note that lithium data are not shown here because the Fe 3p electron binding energies overlap with the Li 1s electron binding energies, making the data difficult to interpret and less meaningful. The C 1s peaks are shown in Figure 5f to illustrate that the largest carbon peak in each sample was shifted to 284.5 eV, and the data for the other elements were shifted by the same amount.

3.4. SEM Characterization. The morphologies of $LiFePO_4$ and $LiFe_{0.85}(VO)_{0.15}PO_4$ were also characterized by SEM, as shown in Figure 6. $LiFePO_4$ forms uniform nanorod particles which have been analyzed by TEM in previous work, in which they were shown to be single crystals with an average size of about 40 nm by 100 nm.[15,17] Conversely, $LiFe_{0.85}(VO)_{0.15}PO_4$ has several types of shapes including rods, plate-like particles, and spheres. The particle size is less uniform as well, but the particles are still at the nano scale.

3.5. Electrochemical Characterization. The vanadyl ion substituted samples were also characterized electrochemically by cyclic voltammetry (CV) to determine the activity of the iron and vanadium redox couples. The CV curves are shown in

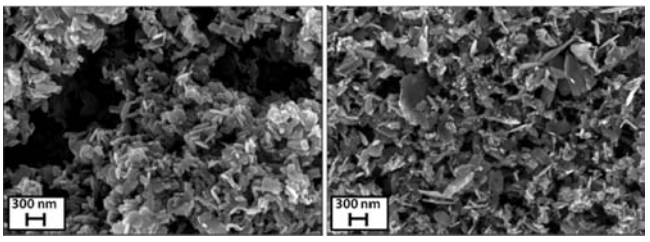

Figure 6. SEM micrographs of $LiFePO_4$ (left) and $LiFe_{0.85}(VO)_{0.15}PO_4$ (right).

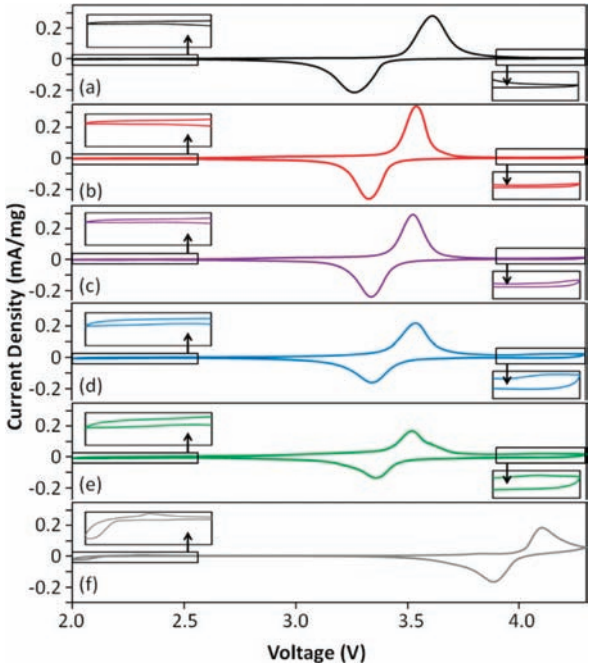

Figure 7. CV data of (a) $LiFePO_4$, (b) $LiFe_{0.95}(VO)_{0.05}PO_4$, (c) $LiFe_{0.90}(VO)_{0.10}PO_4$, (d) $LiFe_{0.85}(VO)_{0.15}PO_4$, (e) $LiFe_{0.75}(VO)_{0.25}PO_4$, and (f) SG $LiVOPO_4$ with the insets showing the regions between 2.0 and 2.6 V as well as 3.9 to 4.3 V.

Figure 7a−f and a summary of the charge and discharge peak locations are presented in Table 4. The second CV cycle is analyzed in detail because the CV peak locations stabilize after one cycle. $LiFePO_4$ has charge and discharge peaks centered around 3.45 V and the SG $LiVOPO_4$ sample has peaks centered around 4.0 V. The samples all have peaks centered around 3.45 V, which correspond to the activity of the $Fe^{2+/3+}$ couple. The vanadyl ion substituted samples also exhibit very broad peaks between 3.9 and 4.3 V that increase in size with increasing x in $LiFe_{1-x}(VO)_xPO_4$. These peaks are illustrated in more detail by the insets (all drawn to equal scale), which are located on the bottom, right corner of each CV plot. The peaks centered at 3.45 V in the vanadyl ion substituted samples are closer together in voltage and less broad than those in $LiFePO_4$, indicating less polarization. Increasing substitution of $(VO)^{2+}$ for Fe^{2+} leads to decreasing iron peak intensity for the peaks centered at 3.45 V and increasing current density in the region between 4.0 and 4.3 V. The latter current density can be attributed to the redox activity of the $V^{4+/5+}$ couple since $LiVOPO_4$ has a peak in the same region. Because of this activity in the region between 3.9 and 4.3 V, we can conclude that the vanadyl ions in the vanadyl substituted samples are redox active. Also, the $Fe^{2+/3+}$ peaks for the vanadyl ion substituted samples systematically shift to higher discharge potentials and lower charge potentials with increasing x in $LiFe_{1-x}(VO)_xPO_4$, as summarized in Table 4.

Table 4. CV Charge and Discharge Peak Voltages of $LiFe_{1-x}(VO)_xPO_4$

compound	$Fe^{2+/3+}$ charge peak voltage (V)	$Fe^{2+/3+}$ discharge peak voltage (V)
$LiFePO_4$	3.62	3.27
$LiFe_{0.95}(VO)_{0.05}PO_4$	3.54	3.33
$LiFe_{0.90}(VO)_{0.10}PO_4$	3.54	3.33
$LiFe_{0.85}(VO)_{0.15}PO_4$	3.53	3.34
$LiFe_{0.75}(VO)_{0.25}PO_4$	3.52	3.36

The SG $LiVOPO_4$ curve also has small peaks close to 2 V. Because this is difficult to see from the scale in the plot, the region between 2.0 and 2.6 V has been expanded in insets shown on the top, left corner of each CV plot. SG $LiVOPO_4$ has been cycled between 2.0 and 4.3 V in this study to be consistent with the $LiFePO_4$ and the other samples tested, but typically $LiVOPO_4$ is cycled between 3.0 and 4.5 V. The activity seen near 2 V in SG $LiVOPO_4$ can be attributed to oxidation and reduction of the $V^{3+/4+}$ couple. $LiVOPO_4$ can accept a second Li^+ ion to form Li_2VOPO_4, which has activity near 2 V.[33−35] It is clear that as x increases, the $LiFe_{1-x}(VO)_xPO_4$ samples also have a small amount of activity near 2 V. The separation between charge and discharge CV curves increases in size with increasing substitution of $(VO)^{2+}$ for Fe^{2+}. Like the activity between 3.9 and 4.3 V, there are not sharp peaks between 2.0 and 2.5 V. However, this activity is still likely attributable to the activity of the $V^{3+/4+}$ couple since Li_2VOPO_4 also shows activity in this voltage range. It should be noted that the Fe_3O_4 impurity was removed with a magnetic stir bar before the electrochemical measurements. Also, even if any trace amount of Fe_3O_4 is present, it will not contribute to the electrochemical performance as the lithium insertion into Fe_3O_4 occurs below 2 V and our electrochemical tests were carried out above 2 V.

Further evidence of vanadium redox activity is evident from the first charge−discharge curves shown in Figure 8a−e with charge and discharge rates of C/10, C/2, and 2C for $LiFe_{1-x}(VO)_xPO_4$. The SG $LiVOPO_4$ is also presented and was cycled at 2.0−4.3 V and 3.0−4.5 V, as shown in Figures 8f and 8g, respectively. The $LiFe_{1-x}(VO)_xPO_4$ curves generally exhibit behavior characteristic of $LiFePO_4$. The capacity is shown to decrease with increasing x in $LiFe_{1-x}(VO)_xPO_4$, which is partially due to the lower theoretical capacity of $LiVOPO_4$ and could be due to iron vacancies as well.

The charge curves exhibit a change in slope around 4 V. They flatten out at higher voltage, and this feature increases in extent with increasing x in $LiFe_{1-x}(VO)_xPO_4$. The capacity at 4 V is present because of the activity of the $V^{4+/5+}$ couple. $LiVOPO_4$ clearly exhibits a plateau at 4 V, as shown in Figures 8e and 8f. It is also clear that the discharge curves for $LiFe_{1-x}(VO)_xPO_4$ have a change in slope at around 2.5 V and flatten out between 2.0 and 2.5 V. This can be attributed to the activity of the $V^{3+/4+}$ couple by comparison to Figure 8f, the curve for SG $LiVOPO_4$.

As x increases, the $LiFe_{1-x}(VO)_xPO_4$ samples also show gradual suppression of the two-phase behavior that is typical for $LiFePO_4$. For $LiFePO_4$, shown in Figure 8a, the two-phase plateau

dx.doi.org/10.1021/ic1025747 |Inorg. Chem. 2011, 50, 3613–3620

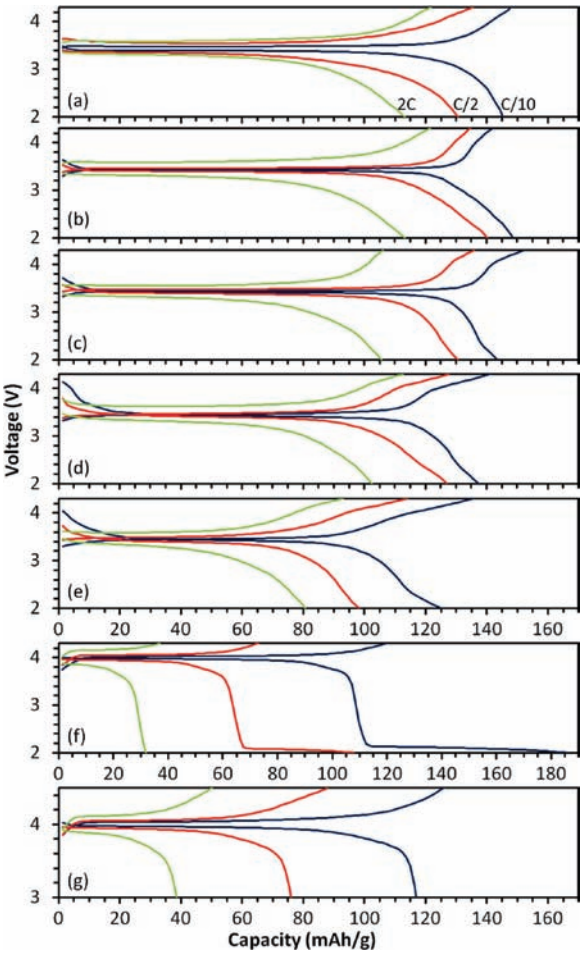

Figure 8. First charge−discharge curves of (a) $LiFePO_4$, (b) $LiFe_{0.95}(VO)_{0.05}PO_4$, (c) $LiFe_{0.90}(VO)_{0.10}PO_4$, (d) $LiFe_{0.85}(VO)_{0.15}PO_4$, (e) $LiFe_{0.75}(VO)_{0.25}PO_4$, and (f) SG $LiVOPO_4$ cycled at 2.0−4.3 V (note change of capacity scale), and (g) SG $LiVOPO_4$ cycled at 3.0−4.5 V.

begins immediately upon discharge, so there is only a very small single-phase region for $LiFePO_4$. For $LiFe_{0.75}(VO)_{0.25}PO_4$, however, there is considerable single-phase behavior at the beginning of the discharge curve, and the two-phase region is decreased greatly.

The suppression of the two-phase behavior is best demonstrated through examination of the open-circuit voltage curve for $LiFe_{0.75}(VO)_{0.25}PO_4$, shown in Figure 9. $LiFePO_4$ is notorious for its very flat voltage curve at 3.45 V. In contrast, the $LiFe_{0.75}(VO)_{0.25}PO_4$ sample exhibits a continuously sloping open-circuit voltage curve. A sloping voltage versus capacity curve suggests a single-phase reaction mechanism, rather than a two-phase mechanism. The sloping voltage curve could be caused by the substitution of $(VO)^{2+}$ for Fe^{2+} or it could be due to iron vacancies in the samples. A single sloping voltage curve for $LiFePO_4$ has been reported previously for a sample with small particle size and 10% iron vacancies, indicating that nonstoichiometry combined with small particles size may lead to single-phase behavior.[36]

Single phase charging and discharging is of interest because it allows for greater coexistence of Fe^{2+} and Fe^{3+} species in the lattice without the presence of a phase boundary. This has rate implications since electronic conductivity in $LiFePO_4$ is achieved

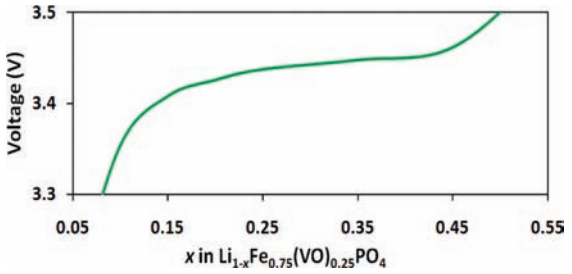

Figure 9. Open-circuit voltage curve of $LiFe_{0.75}(VO)_{0.25}PO_4$.

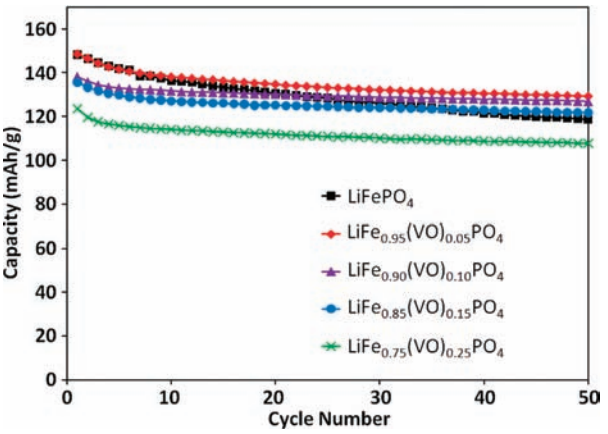

Figure 10. Cycle life data of $LiFe_{1-x}(VO)_xPO_4$ with $0 \leq x \leq 0.25$.

by small polaron hopping of Fe^{3+} holes or Fe^{2+} electrons. These charge carriers increase in concentration in a single-phase system.[37,38] Also, although battery materials with flat voltage curves are beneficial because they can supply power at a constant voltage, sloping charge−discharge curves make state of charge determination easier for batteries.[36]

Although the capacity and rate capability decrease with increasing $(VO)^{2+}$ substitution in $LiFe_{1-x}(VO)_xPO_4$, the capacity retention during extended cycling is better for all of the vanadyl ion substituted samples compared to $LiFePO_4$, as shown in Figure 10. It is possible that the improved cyclability could be due to the iron vacancies in the samples; the iron vacancies may suppress anti-site disorder between lithium and iron, and thereby enhance the lithium diffusivity. By 50 cycles, the capacities of all of the substituted samples except $LiFe_{0.75}(VO)_{0.25}PO_4$ are fairly stable and exceed the capacity of pristine $LiFePO_4$. Because of redox activity at higher voltage and the increased capacity, the energy densities of the vanadyl ion substituted samples are also higher than for $LiFePO_4$ after 50 cycles. It should be noted that all of the data presented here are for samples without any carbon coating, and MW-ST $LiFePO_4$ with carbon coating has been shown before to exhibit very good capacity retention.[15] Therefore, the trend in the cyclability results shown in Figure 10 may differ in the presence of carbon coating.

Finally, the $LiFe_{1-x}(VO)_xPO_4$ samples were made by a unique MW-ST process. The samples are difficult to make by conventional synthesis methods because $LiFePO_4$ generally requires heating in a reducing atmosphere to avoid the oxidation of Fe^{2+}, but $LiVOPO_4$ synthesis generally requires heating in an oxidizing atmosphere. Initial results from heating these $LiFe_{1-x}(VO)_xPO_4$ samples in reducing and oxidizing environments

dx.doi.org/10.1021/ic1025747 |Inorg. Chem. 2011, 50, 3613–3620

show that the vanadyl ion substituted samples are metastable and the phases are difficult to access by conventional methods, as will be discussed in future work.

CONCLUSIONS

We have synthesized vanadyl ion substituted $LiFePO_4$ samples of the form $LiFe_{1-x}(VO)_xPO_4$ with $0 \leq x \leq 0.25$ by a rapid microwave-solvothermal process at less than 300 °C within 10 min. The vanadyl ion substitution in the olivine lattice is evidenced by shifts in XRD and FTIR peaks. XPS data confirm that the oxidation state of vanadium is 4+ in $LiFe_{1-x}(VO)_xPO_4$, and ICP data suggest that iron vacancies are formed upon substituting more than 5% $(VO)^{2+}$ for Fe^{2+}. CV and charge−discharge curves show that vanadium is electrochemically active, and the typical two-phase plateau behavior characteristic to $LiFePO_4$ is found to be suppressed in the vanadyl ion substituted samples. Although the capacity and rate capability decrease with increasing x in $LiFe_{1-x}(VO)_xPO_4$, the cycle life improves; however, the samples examined are not coated with carbon. As will be shown in future work, $LiFe_{1-x}(VO)_xPO_4$ is thermally unstable, and is thus a metastable phase that may be difficult to synthesize by conventional methods.

AUTHOR INFORMATION

Corresponding Author

*E-mail: rmanth@mail.utexas.edu. Phone: 512-471-1791. Fax: 512-471-7681.

ACKNOWLEDGMENT

This work was supported by the Office of Vehicle Technologies of the U.S. Department of Energy under Contract No. DE-AC02-05CH11231. One of the authors (K.H.) thanks the National Science Foundation for the award of a Graduate Research Fellowship. The authors would also like to acknowledge the National Science Foundation for funding the Kratos Axis Ultra XPS used in this work under grant number 0618242 and thank Dr. A. Vadivel Murugan for his keen assistance at the initial stages of the microwave synthesis, Danielle Applestone for her assistance with XPS, and R. K. Harrison for his assistance with SEM analysis.

REFERENCES

(1) Manthiram, A.; Goodenough, J. B. *J. Solid State Chem.* **1987**, *71*, 349.
(2) Manthiram, A.; Goodenough, J. B. *J. Power Sources* **1989**, *26*, 403.
(3) Padhi, A. K.; Nanjundasawamy, K. S.; Goodenough, J. B. *J. Electrochem. Soc.* **1997**, *144*, 1188.
(4) Yamada, A.; Hosoyo, M.; Chung, S.-C.; Kudo, Y.; Hinokuma, K.; Liu, K.-Y.; Nishi, Y. *J. Power Sources* **2003**, *119*, 232.
(5) Li, Z.; Zhang, D.; Yang, F. *J. Mater. Sci.* **2009**, *44*, 2435.
(6) Jugovic, D.; Uskokovic, D. *J. Power Sources* **2009**, *190*, 538.
(7) Gaberscek, M.; Dominko, R.; Jamnik, J. *Electrochem. Commun.* **2007**, *9*, 2778.
(8) Yamada, A.; Chung, S. C.; Hinokuma, K. *J. Electrochem. Soc.* **2001**, *148*, A224.
(9) Ellis, B.; Kan, W. H.; Makahnouk, W. R. M.; Nazar, L . F. *J. Mater. Chem.* **2007**, *17*, 3248.
(10) Wang, Y.; Wang, J.; Yang, J.; Nuli, Y. *Adv. Funct. Mater.* **2006**, *16*, 2135.
(11) Ravet, N.; Chouinard, Y.; Magnan, J. F.; Besner, S.; Gauthier, M.; Armand, M. J. *J. Power Sources* **2001**, *97*, 503.
(12) Park, K.-S.; Schougaard, S. B.; Goodenough, J. B. *Adv. Mater.* **2007**, *19*, 848.
(13) Murugan, A. V.; Muraliganth, T.; Manthiram, A. *J. Electrochem. Soc.* **2009**, *152*, A79.
(14) Muraliganth, T.; Murugan, A. V.; Manthiram, A. *J. Mater. Chem.* **2008**, *18*, 5661.
(15) Murugan, A. V.; Muraliganth, T.; Manthiram, A. *J. Phys. Chem. C* **2008**, *112*, 14665.
(16) Murugan, A. V.; Muraliganth, T.; Manthiram, A. *Electrochem. Commun.* **2008**, *10*, 903.
(17) Murugan, A. V.; Muraliganth, T.; Ferreira, P. J.; Manthiram, A. *Inorg. Chem.* **2009**, *48*, 946.
(18) Whittingham, M. S.; Song, Y.; Lutta, S.; Zavalij, P. Y.; Chernova, N. A. *J. Mater. Chem.* **2005**, *15*, 3362.
(19) Azmi, B. M.; Ishihara, T.; Nishiguchi, H.; Takita, Y. *J. Power Sources* **2003**, *119*, 273.
(20) Azmi, B. M.; Ishihara, T.; Nishiguchi, H.; Takita, Y. *Electrochim. Acta* **2002**, *48*, 165.
(21) Lii, K. H.; Li, C. H.; Cheng, C. Y.; Wang, S. L. *J. Solid State Chem.* **1991**, *95*, 352.
(22) Gaubicher, J.; Le Mercier, T.; Chabre, Y.; Angenault, J.; Quarton, M. *J. Electrochem. Soc.* **1999**, *146*, 4375.
(23) Barker, J.; Saidi, M. Y.; Swoyer, J. L. *J. Electrochem. Soc.* **2004**, *151*, A796.
(24) Ren, M. M.; Zhou, Z.; Su, L. W.; Gao, X. P. *J. Power Sources* **2009**, *189*, 786.
(25) Salah, A. A.; Jozwiak, P.; Zaghib, K.; Garbarczyk, J.; Gendron, F.; Mauger, A.; Julien, C. M. *Spectrochim. Acta, Part A* **2006**, *65*, 1007.
(26) Lemos, V.; Guerini, S.; Filho, J. M.; Lala, S. M.; Montoro, L. A.; Rosolen, J. M. *Solid State Ionics* **2006**, *177*, 1021.
(27) Baran, E. J.; Vassallo, M. B. *J. Raman Spectrosc.* **1994**, *25*, 203.
(28) Bhuvaneswari, M. S.; Selvasekarapandian, S.; Kamishima, O.; Kawamura, J.; Hattori, T. *J. Power Sources* **2005**, *139*, 279.
(29) Fey, G. T.-K.; Cho, Y.-D.; Muralidharan, P. *Pure. Appl. Chem.* **2008**, *80*, 2521.
(30) Silcersmit, G.; Depla, D.; Poelman, H.; Marin, G. B.; De Gryse, R. *J. Electron Spectrosc. Relat. Phenom.* **2004**, *135*, 167.
(31) Dedryvere, R.; Maccario, M.; Croguennec, L.; Le Cras, F.; Delmas, C.; Gonbeau, D. *Chem. Mater.* **2008**, *20*, 7164.
(32) Sarvanan, K.; Reddy, M. V.; Balaya, P.; Gong, H.; Chowdari, B. V. R.; Vittal, J. J. *J. Mater. Chem.* **2009**, *19*, 605.
(33) Whittingham, M. S.; Song, Y.; Lutta, S.; Zavalij, P. Y.; Chernova, N. A. *J. Mater. Chem.* **2005**, *15*, 3362.
(34) Ren, M. M.; Zhou, Z.; Gao, X. P. *J. Appl. Electrochem.* **2010**, *40*, 209.
(35) Song, Y.; Zavalij, P. Y.; Whittingham, M. S. *J. Electrochem. Soc.* **2005**, *152*, A721.
(36) Gibot, P.; Casas-Cabanas, M.; Laffont, L.; Levasseur, S.; Carlack, P.; Hamelet, S.; Tarascon, J.-M.; Masquelier, C. *Nat. Mater.* **2008**, *7*, 741.
(37) Ellis, B.; Herle, P. S.; Rho, Y.-H.; Nazar, L. F.; Dunlap, R.; Perry, L. K.; Ryan, D. H. *Faraday Discuss.* **2007**, *134*, 119.
(38) Ellis, B.; Perry, L. K.; Ryan, D. H.; Nazar, L. F. *J. Am. Chem. Soc.* **2006**, *128*, 11416.